AGU PUBLICATIONS

Geochemistry, Geophysics, Geosystems

RESEARCH ARTICLE
10.1002/2015GC006050

Key Points:
- Tectonically induced reactivation of recalcitrant organic matter
- Methane C-isotopes can delineate locations of active microbial processes
- Time constraint on earthquake-related transient temperature increase

Supporting Information:
- Supporting Information S1

Correspondence to:
N. Riedinger,
Natascha.Riedinger@okstate.edu

Citation:
Riedinger, N., M. Strasser, R. N. Harris, G. Klockgether, T. W. Lyons, and E. J. Screaton (2015), Deep subsurface carbon cycling in the Nankai Trough (Japan)—Evidence of tectonically induced stimulation of a deep microbial biosphere, *Geochem. Geophys. Geosyst.*, *16*, 3257–3270, doi:10.1002/2015GC006050.

Received 6 AUG 2015
Accepted 4 SEP 2015
Accepted article online 10 SEP 2015
Published online 26 SEP 2015

Deep subsurface carbon cycling in the Nankai Trough (Japan)—Evidence of tectonically induced stimulation of a deep microbial biosphere

N. Riedinger[1,2,3], M. Strasser[4,5], R. N. Harris[6], G. Klockgether[7], T. W. Lyons[1], and E. J. Screaton[8]

[1]Department of Earth Sciences, University of California - Riverside, Riverside, California, USA, [2]Formerly at Max Planck Institute for Marine Microbiology, Bremen, Germany, [3]Now at Boone Pickens School of Geology, Oklahoma State University, Stillwater, Oklahoma, USA, [4]Geological Institute, ETH Zurich, Zurich, Switzerland, [5]Now at Institute of Geology, University of Innsbruck, Innsbruck, Austria, [6]College of Oceanic and Atmospheric Sciences, Oregon State University, Corvallis, Oregon, USA, [7]Max Planck Institute for Marine Microbiology, Bremen, Germany, [8]Department of Geological Sciences, University of Florida, Gainesville, Florida, USA

Abstract The abundance of microbial life and the sources of energy necessary for deep subsurface microbial communities remain enigmatic. Here we investigate deep microbial processes and their potential relationships to tectonic events in sediments from the Nankai Trough offshore Japan, drilled and sampled during IODP (Integrated Ocean Drilling Program) Expedition 316. Observed methane isotope profiles indicate that microbially mediated methane production occurs at Sites C0006 and C0007 in sediments below ~450 meters below seafloor (mbsf) and ~425 mbsf, respectively. The active carbon cycling in these deep subsurface sediments is likely related to the highly dynamic tectonic regime at Nankai Trough. We propose that transient increases in temperature have restimulated organic matter degradation at these distinct depths and explore several candidate processes for transient heating. Our favored hypothesis is frictional heating associated with earthquakes. In concert with transient heating leading to the reactivation of recalcitrant organic matter, the heterogeneous sedimentary system provides niches for microbial life. The newly available/accessible organic carbon compounds fuel the microbial community—resulting in an onset of methanogenesis several hundred meters below the seafloor. This process is captured in the methane C-isotope signal, showing the efficacy of methane C-isotopes for delineating locations of active microbial processes in deeply buried sediments. Additionally, simple model approaches applied to observed chemical pore water profiles can potentially constrain timing relationships, which can then be linked to causative tectonic events. Our results suggest the occurrence of slip-to-the-trench earthquake(s) 200–400 year ago, which could relate to historical earthquakes (1707 Hoei and/or 1605 Keicho earthquakes).

1. Introduction

Most biogenic hydrocarbon gases in marine sediments are produced in organic-rich areas as a direct consequence of microbial activity under anaerobic conditions [*Martens and Berner*, 1974]. The dominant fraction of these gases is methane (≥99%), assumed to be produced from organic matter mineralization over a specific depth interval below the sulfate methane transition (SMT)—a few centimeters to tens of meters below the seabed. Typically, generation of biogenic gas is associated with fine-grained sediment due to its characteristically higher initial organic content. The quality and thus bioavailability of the organic matter can influence the spatial patterns of methane production [*Canfield*, 1994] in marine sediments, and the carbon isotopes of both CH_4 and dissolved inorganic carbon (DIC), as records of methanogenesis, increase with the deposition rate of reactive marine organic matter [*Blair*, 1998]. At greater depths, microbial organic matter degradation generally ceases, as the bioavailability of the residual organic pool declines, leading to an absence of methanogenesis [*Sivan et al.*, 2007]. This observation can be explained by site-related parameters such as the composition of the organic matter and/or the type of microbial community present. In general, organic matter in these deep (several tens to hundreds of meters) subsurface sediments is thought to be resistant to biodegradation [e.g., *de Leeuw and Largeau*, 1993; *Hedges and Keil*, 1995] and cannot fuel appreciable metabolic activity in deep subsurface environments.

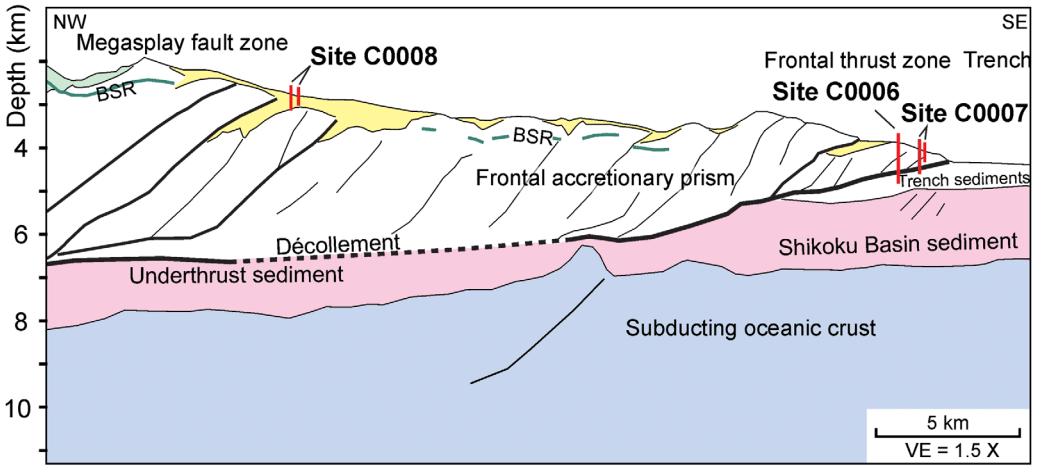

Figure 1. Simplified structural overview of the frontal thrust region including IODP316 drilling locations and bottom-simulating reflector (BSR) [after *Moore et al.*, 2009, 2015].

However, additional sources of energy are thought to overcome depth limitations so that microbial activity can proceed in sediments several hundred meters beneath the seabed [e.g., *Parkes et al.*, 1990; *Jørgensen and D'Hondt*, 2006; *Yoshioka et al.*, 2009]. These additional sources of energy may come from hydrogen derived from various chemical processes such as the chemical alteration of young basaltic crust or the decay of natural radionuclides [*Holm and Charlou*, 2001; *Lin et al.*, 2005]. However, increasing temperature with depth, such as with increasing burial depth, can activate chemical alteration of minerals [*Surdam and Crossey*, 1985] or (re)activate buried organic matter to supply the deep biosphere with energy [*Wellsbury et al.*, 1997; *Parkes et al.*, 2006; *Roussel et al.*, 2008; *Burdige*, 2011].

Due to its depositional and dynamic tectonic setting, the Nankai Trough, offshore Japan, is ideal for studies focused on the interplay between the carbon cycle and the deep biosphere [e.g., *Riedinger et al.*, 2010]. Frontal accretion, uplift, and internal deformation of trench wedge and underlying Shikoku Basin sediments are the results of subduction of the Philippine Sea plate below southwest Japan [*Underwood et al.*, 2003; *Strasser et al.*, 2009; *Moore et al.*, 2015]. This setting is characterized by a complex lithostratigraphy and depositional history. Thrust faults and interbedded gravels and sands deposited in the axial trench and uplifted in the frontal prism can influence the degree of reactive mineral alteration. Varying sedimentation rates, sediment composition, organic matter content, and availability of reactive minerals dramatically affect the oxidative capacity and permeability of sediments [e.g., *Dugan and Daigle*, 2011; *Rowe et al.*, 2011].

Here we present results for carbon geochemistry of the upper slope of the Nankai Trough accretionary prism at Integrated Ocean Drilling Program (IODP) Site C0008 and from the toe of the slope at IODP Sites C0006 and C0007. Our results include the carbon and hydrogen isotope composition of methane (CH_4). The dynamic nature of the Nankai accretionary wedge directly juxtaposes various redox environments and their corresponding geochemical gradients. As a result, this region is of high interest for carbon cycle studies in deep biosphere environments.

2. Site Description and Methods

2.1. Sedimentary Setting

Sediment and gas void samples for methane analyses were collected during IODP Expedition 316 on the D/V Chikyu, from Hole C0008A (33°12.8229′N, 136°43.5997′E), located in a slope basin of the upper slope of the accretionary wedge at 2751 m water depth. Samples were also collected from Holes C0006E (33°01.6444′N, 136°47.6282′E), C0006F (33°01.6242′N, 136°47.6282′E), and C0007D (33°01.3167′N, 136°47.8872′E) along the prism toe at water depths of 3875.8 m, 3875.5 m, and 4049.0 m, respectively (Figure 1).

Two major lithologic units were recovered at Site C0008, and three and four major units were recovered at Sites C0006 and C0007, respectively (Figure 1) [*Kinoshita et al.*, 2009; *Screaton et al.*, 2009a, *Screaton et al.*, 2009b; *Strasser et al.*, 2009; *Underwood and Moore*, 2011]. At Site C0008, Unit I consists of a Pliocene-to-

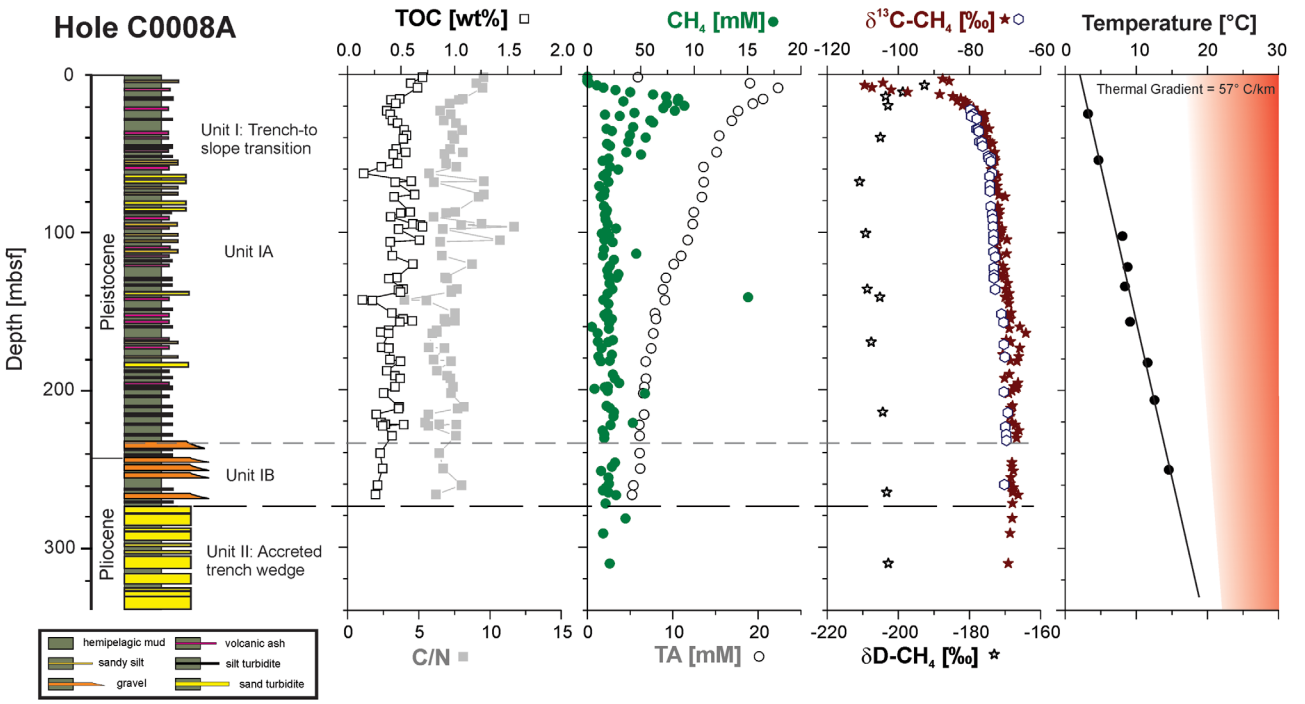

Figure 2. The carbon isotope signal of methane (δ^{13}C-CH_4) measured in void gas samples (open blue circles) from Hole C0008A is in good agreement with headspace methane (red stars) data. Both results point to the main methane production horizon between 8 and 30 mbsf. The high methane (CH_4) concentration outlier can be related to the occurrence of gas hydrates [*Kinoshita et al*., 2009]. Lithostratigraphy, total organic carbon (TOC), TOC to total nitrogen ratios (C/N ratio), methane, total alkalinity (TA) concentration data, and temperature values are shipboard data from IODP Expedition 316 [*Kinoshita et al*., 2009]. Temperature gradient as discussed by *Harris et al*. [2011]. The red zone in the temperature panel suggests the necessary temperature increase for potential organic matter reactivation related to burial (see text for further discussion).

recent slope basin sedimentary succession (Figure 2). At Site C0006, the Pleistocene-to-recent Unit I is characterized by a fining-upward succession of hemipelagic silty clay with interbedded thin sand beds and volcanic ash layers interpreted as a trench-to-slope transition. Deposition occurred on the lowermost slope above the trench floor by hemipelagic settling and postdates accretion of the lower slope site. Unit II is an accreted trench wedge facies with sandy turbidities, gravel, and hemipelagic mud. Unit II is of Pleistocene age at Sites C0006 and C0007 with a coarsening upward trend, in contrast to its Pliocene age at Site C0008. At Site C0006, the succession is structurally complex, with numerous thrust faults causing significant stratigraphic repetition (Figure 3). Unit II is interpreted as having been deposited in a trench setting, with increasing proximity to the axial portion of the trench up section. This stratigraphic succession was accreted about half a million years ago to form the lower trench slope near the toe of the present-day accretionary prism [*Screaton et al*., 2009b]. Unit III represents deep-marine basin sediments with alternating beds of mudstone and sandstone. It is of early Pleistocene to late Miocene age at Site C0006 (below 450 mbsf); no Miocene deposits were observed at Site C0007 (355–435 mbsf) (Figure 4). The silty clay of Unit III was deposited by hemipelagic settling along with accumulation of volcanic ash during major volcanic eruptions. Bioturbation is widespread in these deposits, particularly in the upper part of Unit III. The base of Unit III is marked by a large fault zone that defines the plate boundary fault, along which the unit was accreted [*Screaton et al*., 2009a; *Sakaguchi et al*., 2011]. Below the fault zone at Site C0007, deposits consist mainly of fine-to-medium grained, unconsolidated sand. This Unit IV of Pleistocene age is interpreted as the underthrust part of the trench wedge [*Kinoshita et al*., 2009].

2.2. Analytical Procedures

Total organic carbon (TOC) content was calculated as the difference between total carbon (TC) and inorganic carbon (IC). IC concentrations were measured using a Coulometrics 5012 CO_2 coulometer. TC and total nitrogen concentrations were determined using a Thermo Finnigan Flash EA 1112 CHNS analyzer. TOC is given in weight carbon per dry sediment. Alkalinity was determined by Gran titration. For methane analyses, 3 cm^3 sediment samples were collected with a cutoff syringe. A cork borer was used to take the sample from lithified sediments. In both cases, the samples were extruded into a He-flushed 20 mL glass serum vial

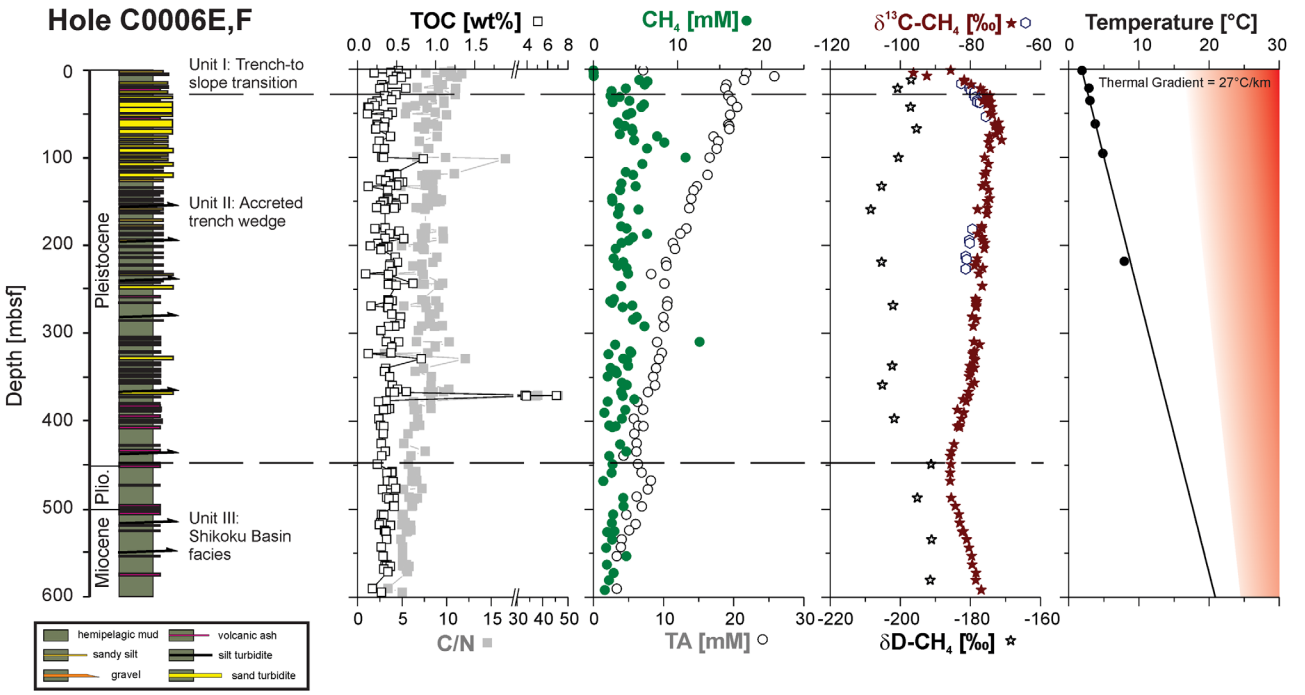

Figure 3. Methane carbon isotopes (δ^{13}C-CH_4) at Holes C0006E and C0006F show a decrease in the isotope signal at around 450 mbsf concurrent with a jump in the total alkalinity (TA) concentration and an increase in the hydrogen isotopes of methane (δD-CH_4). The data indicate onset of active methanogenesis at these deep subsurface sediments. The high methane (CH_4) concentration outlier at ~300 mbsf can be related to the occurrence of gas hydrates [*Kinoshita et al*., 2009]. Lithostratigraphy, total organic carbon (TOC), TOC to total nitrogen ratios (C/N ratio), methane, TA concentration data, and temperature values are shipboard data from IODP Expedition 316 [*Kinoshita et al*., 2009]. Temperature gradient as discussed by *Harris et al*. [2011]. The red zone in the temperature panel suggests the necessary temperature increase for potential organic matter reactivation related to burial (see text for further discussion).

containing 10 mL of 4% NaOH. Void gas samples were collected from observed gas pockets to complement the headspace analyses. Samples were collected directly from gas voids by penetrating the core liner and using a gastight syringe. Methane analyses were performed using an Agilent 6890N gas chromatograph instrument equipped with a flame ionization detector [e.g., *Pimmel and Claypool*, 2001]. The gas concentrations were analyzed relative to five different certified gas standards with variable quantities of low molecular weight hydrocarbons with a precision better than 1%. The concentration of methane in interstitial water was derived from calibrated chromatographic response using the equation described by the *Shipboard Scientific Party* [2003]. The concentrations were subsequently corrected for sediment porosity. All solid-phase carbon and nitrogen measurements, as well as those for the pore waters, were carried out onboard the DV Chikyu [*Kinoshita et al*., 2009].

The stable isotope composition of methane was obtained at the Max Planck Institute for Marine Microbiology, Bremen, Germany, using a Hewlett Packard 6890 GC equipped with a 25 m × 0.32 mm × 0.5 μm CP-Porabond Q (CP7351) column coupled to a ThermoFinnigan Delta Plus XP isotope ratio mass spectrometer (IRMS) via a combustion interface-III. Gas samples (250–1000 μL) were taken from the headspace of the sample vial using a gastight syringe and the solution replacement technique. The stable carbon isotope composition of calcium carbonate ($\delta^{13}C_{carb}$) was measured using a Delta Plus XP IRMS. Carbon and hydrogen isotope ratios are reported in delta notation relative to Vienna Pee Dee Belemnite Standard (VPDB) and Vienna Standard Mean Ocean Water (VSMOW), respectively. The standard deviation (1σ) of replicate measurements was better than 0.8‰ for δ^{13}C-CH_4, 3‰ for δD-CH_4, and 0.2‰ for $\delta^{13}C_{carb}$.

2.3. Numerical Modeling

To model the alkalinity pore water profile, we used the numerical transport and reaction model CoTReM [*Adler et al*., 2001]. A detailed description of this computer software is given in *Adler et al*. [2001] and *Hensen et al*. [2003]. The modeled thickness of 600 m was subdivided into cells of 4 m thickness (dx). The time step to fulfill numerical stability was set to 1 year. We used the measured porosity of the sediment profile [*Screaton et al*., 2009a] and a modern sedimentation rate of 4 cm kyr^{-1} [e.g., *Harris et al*., 2011]. Transport

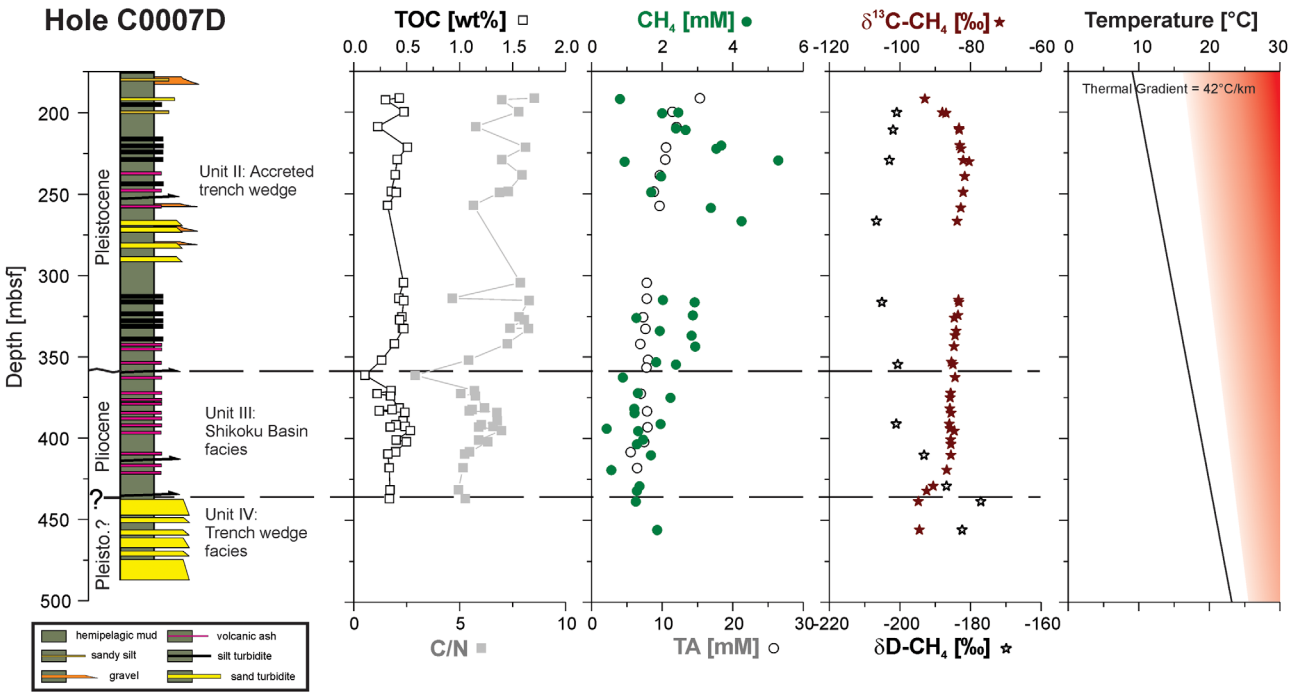

Figure 4. The carbon isotope signal of methane (δ^{13}C-CH_4, red stars) from Hole C0007D displays a strong depletion in ^{13}C at about 425–430 mbsf, while δD-CH4 gets enriched (open stars). Lithostratigraphy, total organic carbon (TOC), TOC to total nitrogen ratios (C/N ratio), methane, and total alkalinity (TA) concentration data are shipboard data from IODP Expedition 316 [*Kinoshita et al*., 2009]. Temperature gradient as discussed by *Harris et al*. [2011]. The red zone in the temperature panel suggests the necessary temperature increase for potential organic matter reactivation related to burial (see text for further discussion).

mechanisms were molecular diffusion in the sediment (D_s) for all solutes in the pore water and advection via sedimentation (burial) for the solid phase and pore water. For the deeper sediments, diffusion coefficients were corrected for tortuosity [*Boudreau*, 1997] and a temperature of 18°C. For geochemical reactions, zeroth-order kinetics was used by defining maximum reaction rates.

As starting conditions, the measured alkalinity concentrations were fit with a smooth curve, and in situ consumption and production rates were applied—both obtained via the application of a Rate Estimation from Concentrations (REC) model [*Lettmann et al*., 2012]. This numerical model applies a smoothing parameter, λ, based on Tikhonov regularization (for further details see *Lettmann et al*. [2012]). The production of alkalinity was simulated by assuming a net equation of 1 mol methane and 1 mol alkalinity produced via 2 mol organic matter. More specific details concerning the parameterization and data handling are given in the respective sections below.

3. Results and Discussion

The sediments at Hole C0008A show low concentrations of TOC (<0.75 wt %) and C/N ratios less than 10 (Figure 2). The latter are indicative of the mainly marine origin of the organic matter. Due to the microbial degradation of organic matter in the uppermost sediment layers, the alkalinity increases with depth. At the sulfate-methane transition (SMT) at about 6 mbsf, total alkalinity (TA) displays its highest values, fueled additionally by anaerobic oxidation of methane. Below this zone, the TA concentration decreases again with depth [*Expedition 316 Scientists*, 2009], indicating no further release of alkalinity into the pore water. The methane concentration and isotope profile at Hole C0008A indicate that the main methane production zone lies below the SMT at depths between 8 and 30 mbsf. Here the δ^{13}C-CH_4 isotopes show the most negative signal (−110‰). Below about 30 mbsf, only minor amounts of methane in the range of a few micromoles are produced. The result is only a very small impact on the isotope signal of the methane and no overall influence on its net concentration. Above the SMT, ^{13}C-CH_4 isotopes are more enriched due to the oxidation of methane and associated fractionation. Similar to Site C0008, quasi steady state methane isotope profiles have been reported from the Gulf of Mexico (Site U1325) [*Pohlman et al*., 2009], indicating that

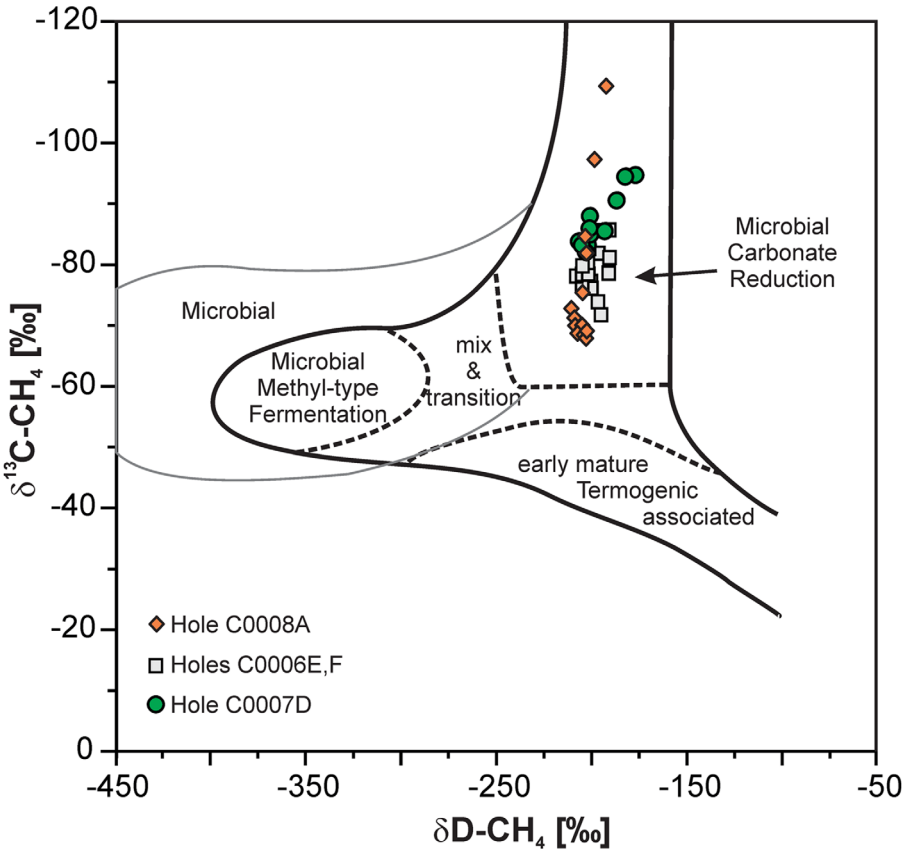

Figure 5. Methane isotope classification diagram modified after *Whiticar* [1999]. The isotope data for Site C0006 (gray squares), and Holes C0007D (green-filled circles) and C0008A (orange rectangles) point to hydrogenotrophic carbonate reduction as the main methane production pathway.

our profile distributions are not unique. Importantly, the occurrence of gas hydrates in sediments at Hole C0008A [see *Kinoshita et al*., 2009] and its dissociation during sampling does not seem to impact the carbon isotope signal of methane in these sediments—no change in the δ^{13}C-CH_4 composition was observed throughout the core where gas hydrates remains were detected—but might have an influence on the hydrogen isotope composition (Figure 2). This inference is supported by gas void isotope values that mimic the trend of the headspace carbon isotope composition, with only slight depletion (1–3‰) but an overall less scattered signal compared to the headspace samples (Figure 2). Generally, the carbon isotope signal shows a self-consistent signal, especially compared to the methane concentration profile, which is vulnerable to loss of methane during sampling.

Similar to the deposits at Site C0008, the sediments at Holes C0007D, C0006E, and C0006F show low concentrations of TOC throughout the core, with average values of 0.39 and 0.46 wt %, respectively. The C/N ratios are mostly less than 10, consistent with a dominantly marine origin of the organic matter. Isotope data for the hydrogen and carbon of the methane range between −100 and −70 for δ^{13}C-CH_4 and −210 and −170 for δD-CH_4, which are indicative of its microbial origin (Figure 5). These isotope data are diagnostic of in situ methane formation, with hydrogenotrophic CO_2 reduction as the main formation pathway [*Whiticar et al*., 1986]. *Yoshioka et al*. [2009] and *Inagaki et al*. [2015] showed that over several hundreds to thousands of meters sediment depth, methanogenesis can proceed at low rates, with CO_2 reduction as the main production pathway. Preferential utilization of ^{12}C by methanogens leaves the residual inorganic carbon enriched in ^{13}C, and thus with increasing depth the DIC and the methane become progressively enriched in ^{13}C [*Whiticar*, 1999]. Furthermore, preferential use of the lighter isotope ^{12}C during anaerobic oxidation of methane (AOM) is capable of enriching the residual methane in ^{13}C [*Alperin et al*., 1988]—explaining the δ^{13}C trend we observe at the sulfate methane transition (SMT).

In contrast to Site C0008, which shows methane production just below the SMT at around 7 mbsf, data at the frontal thrust sites indicate additional methane production in the deeper subsurface. At Site C0007, the methane concentration and isotope profiles indicate that the main methane production zone is between depths of 175 and 225 mbsf, well below the SMT. Between 225 and 425 mbsf, none or only small amounts of methane are produced, with a very small impact on the isotope signal and no overall influence on the net concentration of methane (Figure 4). Below about 425 mbsf, the methane isotope composition changes abruptly where δ^{13}C values become more negative and hydrogen isotopes are more positive. The contemporaneous increase in methane concentration and decrease of ^{13}C-CH_4 suggests production of methane from a carbon pool that contains light carbon isotopes (Figure 4). Similar to the observed deep subsurface isotope excursion at Site C0007, the sediments at Site C0006 show an offset in the methane carbon isotope profile at around 450 mbsf (within the upper part of Unit III).

Methane carbon isotope profiles similar to those we observe in the Nankai Trough were also reported from two sites in the Gulf of Mexico [*Pohlman et al*., 2009]. At these sites, a shift in the isotope values in the deep sediments was observed at the depth of the bottom-simulating reflector concurrent with a porosity change to higher values, which can provide space for the microbial communities [*Inagaki et al*., 2003]. However, the reported isotope values for the two cores from the Gulf of Mexico show a trend to thermogenic methane formation and a homogenous δD-CH_4 isotope profile. These relationships differ from our observations at Sites C0006 and C0007, which indicate microbial methane formation (Figure 5) and variations in the observed δD values (Figure 4).

3.1. Candidate Explanations of Observed Carbon Isotope Shift

Here we examine several alternative explanations for the observed methane carbon isotope shift such as methane oxidation, change of the substrate, or alternative CO_2 sources. While the process of anaerobic oxidation of methane (AOM) usually leads to an enrichment of ^{13}C in the residual methane [e.g., *Alperin et al*., 1988], a recent study by *Yoshinaga et al*. [2014] suggested that anaerobic oxidation of methane via sulfate reduction (SR-AOM) can lead to depletion in the stable carbon isotope signal. More specifically, the authors' in vitro experiments showed ^{13}C depletion at low sulfate concentrations. It follows from these experiments that this diagnostic isotopic expression requires the presence of sulfate concentrations in pore fluids. Production and immediate consumption of sulfide might limit the availability of sulfate in the pore fluids; however, the process should lead to the accumulation of sulfide in the pore fluids, which was not observed [*Screaton et al*., 2009b], or to the formation of abundant pyrite at this specific sediment depth. Such a correlation between distinct pyrite enrichment [see *Riedinger and Brunner*, 2014] and the shift in the methane δ^{13}C was also not found. Additionally, SR-AOM should lead to the formation of highly depleted calcium carbonate precipitation, which is not observed in the bulk carbonate stable C-isotopes at Site C0007. In fact, these data show a change from δ^{13}C-Carb $-3.0‰$ (431.6 mbsf) to $-1.9‰$ (437 mbsf). These arguments let us rule out anaerobic oxidation of methane via sulfate reduction.

Methane production can also occur without the presence of organic matter, if H_2 and CO_2 are available. H_2 could be produced mechanochemically or mechanoradically during earthquake rupture [e.g., *Yamaguchi et al*., 2011; *Hirose et al*., 2011]. Earthquake rupture-related mechanochemically H_2 production would lead to a pulse of H_2 formation and thus limiting methanogenesis to very confined temporal and spatial scales. While methanogens require a minimum level of H_2 to produce methane via CO_2 reduction, concentrations below this level suppress methanogenesis [e.g., *Lovley et al*., 1982]. Although this process would provide the energy source for the microbes to produce methane consistent with the observed isotope signature, we would still need a source of dissolved inorganic carbon (DIC) with an isotopic composition that differs from the background DIC. Thus, we need a source of isotopic light carbon to explain the isotopic light methane. This process would decrease the available carbonate pool—inconsistent with the observed alkalinity profile at Site C0006 (Figure 3).

It could also be argued that dissolution of carbonate minerals in deep subsurface sediment could explain the increase in the alkalinity and provide a source of CO_2 depleted in ^{13}C. However, the pore water Ca concentration profile shows a continuous increase with depth and no concentration enrichment peak in correlation with the alkalinity peak can be observed. The Ca-concentrations increase in pore water in the deep sediments at Site C0006 is most likely the result of low-temperature deep subsurface diagenetic reactions such as (volcanic) ash alteration and not related to carbonate dissolution. This interpretation is supported

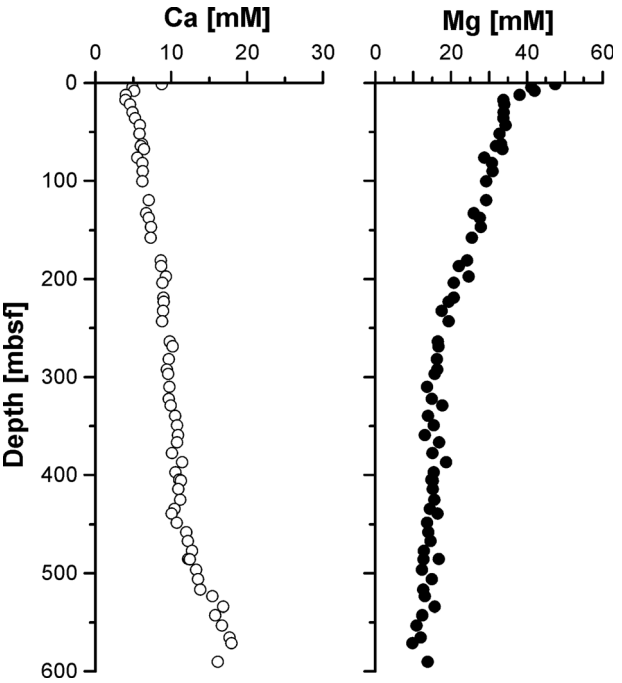

Figure 6. The calcium concentration pore water profile at Holes C0006E and C0006F shows an increase with depth in the deeper sediment layers, while the magnesium concentration decreases. Pore water concentration data are shipboard data from IODP Expedition 316 [*Kinoshita et al*., 2009].

by the inverse trend of the magnesium profile compared to the Ca profile (Figure 6) [*Expedition 316 Scientists*, 2009], suggesting an exchange of Ca and Mg during mineral alteration [e.g., *Gieskes and Lawrence*, 1981]. Therefore, carbonate dissolution as a source for the DIC in this sediment depth can most likely be ruled out.

Having challenged processes such as a source of CO_2 due to carbonate dissolution, or an isotope shift due to methane oxidation, we propose that the onset of microbial methane production via the CO_2-reduction pathway related to organic matter reactivation is the most probable process causing the observed isotope pattern. This possibility is supported by elevated alkalinity in the pore water that coincides with the shift in the carbon isotope composition at Site C0006 (Figure 3), implying that organic matter is microbially mineralized with a consequent production of methane and CO_2. Furthermore, the carbon isotope signal suggests that the reactivated organic matter has a different primary isotopic signature compared to the overlying organic pool. This interpretation is consistent with the variations in the C/N ratio (Figure 3), pointing to a different type of organic matter composition or preservation in this zone [e.g., *Pohlman et al*., 2009].

3.2. Time Constraints

The trend for the isotope composition indicates that the causative event is related to a transient event of young age. More specifically, if methane was continuously produced over a long period of time, diffusive transport would have erased variations in the isotope composition at different depths—unlike what we observe. Here we apply a numerical model to geochemical constituents to investigate the time constraint for the onset of our hypothesized organic matter reactivation. The measured hydrogen and carbon isotope data for methane indicate that methane is microbially produced (Figure 5). Methane production from organic matter occurs via a net reaction for the carbonate reduction pathway (fermentation: $2CH_2O + 2H_2O \rightarrow 2CO_2 + 4H_2$ and carbonate reduction: $CO_2 + 4H_2 \rightarrow CH_4 + 2H_2O$ $+CO_2$): $2CH_2O \rightarrow CO_2 + CH_4$, or via acetate fermentation: $CH_3COOH \rightarrow CO_2 + CH_4$, where for each mol methane produced 1 mol CO_2 is also produced [e.g., *Whiticar et al*., 1986; *Whiticar*, 1999; *Pohlman et al*., 2009]. Because of potential loss of methane during core retrieval (degassing of methane due to pressure changes) [see *Wallace et al*., 2000], methane concentration profiles are not suitable for transport and reaction modeling. Instead, based on the above described relationship of methane and carbonate production by organic matter decomposition processes and an interrelated increase in total alkalinity [e.g., *Emerson et al*., 1982; *Wolf-Gladrow et al*., 2007], we used the concentration profile of total alkalinity to infer the onset of mechanisms affecting methane production in these deep subsurface sediments.

To characterize the zones of current net in situ consumption and production and specifically estimate rates, we use a one-dimensional numerical procedure (REC) [*Lettmann et al*., 2012] to simulate the observed alkalinity concentration profile (Figure 7a). These rates and zones were then implemented in the transport and reaction model (Figure 7). For zones where consumption occurs, the rates were simplified as zero production rates for further approaches. Inferred in situ rates (1.44 pmol cm^{-3} d^{-1}) were used for the surface alkalinity production. For all other depth intervals, background production rates (set in relation to the amount of TOC and C/N ratio) were set <0.01 pmol cm^{-3} d^{-1}. Those rates are in good agreement with previous

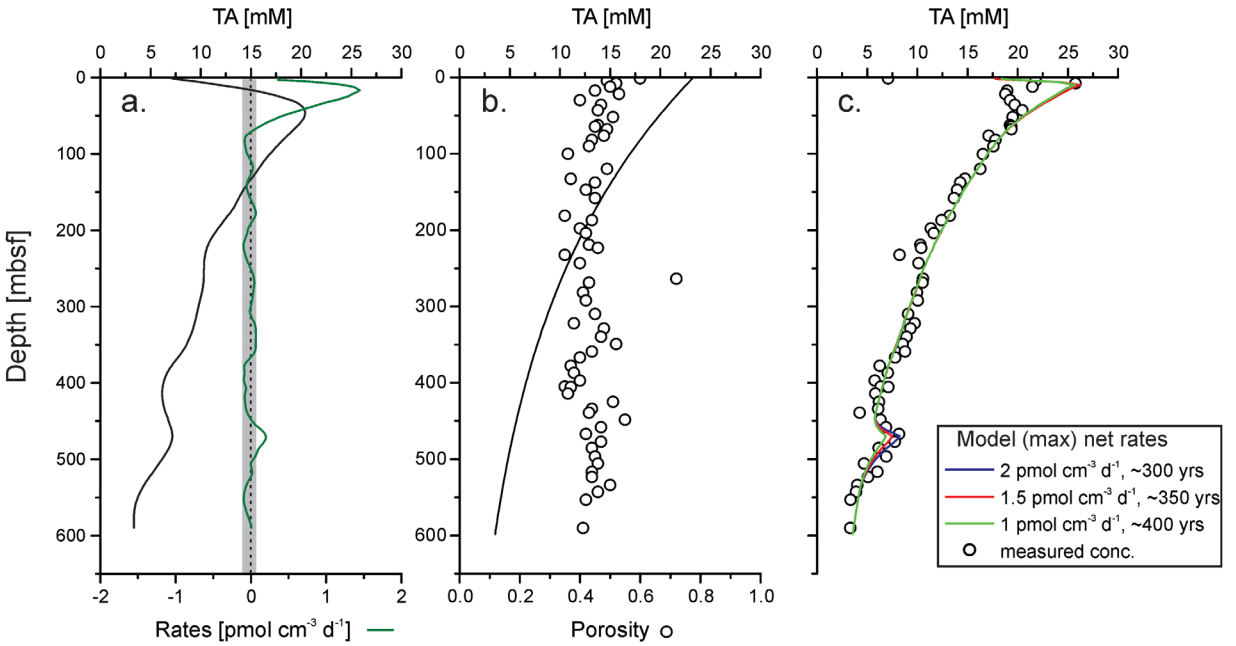

Figure 7. Numerical model data for Site C0006. (a) In situ maximum rates inferred from REC model (green line) and related modeled total alkalinity (TA) profile. (b) Measured porosity data (open circles) (shipboard data from IODP Expedition 316) [*Kinoshita et al.*, 2009] and starting alkalinity concentrations for applied reaction and transport modeling (CoTReM). (c) Measured total alkalinity data (open circles) and modeled total alkalinity concentration profile for different starting maximum net rates. The data show a best model fit for 1.5–2 pmol cm^{-3} d^{-1} with a time of 300 years (only small variation between 200 and 400 years). Lower rates, <1.5 pmol cm^{-3} d^{-1}, are not sufficient to reach measured concentrations even when run for longer period (for further details see text).

reported potential methanogenesis background rates, for example, from the Bering Sea at similar deep subsurface sediments [*Wehrmann et al.*, 2011]. To reconstruct a timeframe for the onset of organic matter reactivation via a temperature increase, we assume that the reactivated organic matter is degraded exponentially (according to *Westrich and Berner* [1984]). The zone with maximum increase of production rates was set at ~470 mbsf, the center of the deep subsurface total alkalinity and δ^{13}C-CH_4 excursion. Assuming that the impact is local at smaller scale (see discussion 3.3 for thermal increase mechanisms), the rates strongly decrease (polynomial reduction) about 30 m below and above this zone. As starting production rates at the time of the event, a series of maximum net rates were applied ranging from 0.3 to 3 pmol cm^{-3} d^{-1}. These starting rates are in the range of reported rates for deep subsurface methanogenesis for the Nankai Trough region off Shikoku Island [*Newberry et al.*, 2004], Hydrate Ridge [*Arning et al.*, 2011], and the West African Margin area [*Sivan et al.*, 2007]. As a limit for the lowest rate at this zone, we chose a current in situ rate of ~0.2 pmol cm^{-3} d^{-1} inferred from the REC model (Figure 7a).

A best model fit to the measured total alkalinity concentration profile was achieved using starting maximum rates of 1.5–2 pmol cm^{-3} d^{-1} (Figure 7c). These rates resulted in the observed profile after approximately 300–350 years (with only small variation between 200 and 400 years before diffusive decrease occurs). High starting rates of 2.5–3 pmol cm^{-3} d^{-1} reached the measured concentration after about 50–150 years, respectively. After a diffusive decrease in concentration, the present-day modeled in situ rates were reached 150–200 years later. Starting rates lower than 1.5 pmol cm^{-3} d^{-1} were not sufficient to reach measured concentrations of total alkalinity. Those lower rates reach their peak concentration after about 400 years before declining again due to diffusive overprint. These maximum concentrations are still below the measured concentration. Our modeling results suggest that a potential causative event most likely occurred in the last 200–400 years, leading to the reactivation of the organic matter and consequent onset of methanogenesis with rates >1.5 pmol cm^{-3} d^{-1}.

3.3. Potential Mechanisms for Transient Thermal Increase Over a Distinct Depth Interval

Having ruled out other methane production models and solved for the timing of hypothesized reactivation of organic matter, we now need to explore the possible driving mechanisms for this reactivation. Microbial methane mediation in sediments below ~450 and ~425 mbsf at IODP Sites C0006 and C0007, respectively,

is unexpected and requires an explanation. Here we explore geochemical and thermal processes that might explain our observations.

Thermal processes offer a viable class of candidate processes because an increase in temperature can make the organic matter available for microbial degradation. *Burdige* [2011] showed that organic matter, refractory at low temperature, can bypass extensive remineralization in shallow sediments and become available for microbial processes with increasing depth and thus increasing temperature. This progressive burial and attendant heating would result in an almost linear change in the bioavailability of organic matter (until a certain time-temperature threshold where the remaining organic material is no longer bioavailable) and not in a sudden excursion in potentially related geochemical constituents as observed in our sediments at the toe of the accretionary prism (Figures 3 and 4). Additionally, Site C0006 is characterized by a low thermal gradient (Figure 3) [*Kinoshita et al*., 2009; *Harris et al*., 2011]. An increase in temperature with depth along the observed geothermal gradient would be too low to account for the reactivation of organic matter at this site (the red zone in Figure 3 shows the approximate temperature required for reactivation; inferred from *Parkes et al*. [2006]). Instead, a transient increase in temperature with a consequent reavailability of the organic matter could be responsible for the observed geochemical signals. Possible processes include advective fluid flow or frictional heating from a nearby fault. Advective fluid flow from deeper layers along the décollement could lead to an increase in temperature; however, there is no clear geochemical evidence for long-distance advective flux of fluids along the décollement and associated splay faults at the sites drilled during Expedition 316 [*Screaton et al*., 2009a].

In contrast to the progressive heating with burial, coseismic frictional heating, as documented at other subduction margins, can lead to a rise in the temperature over a short period of time [e.g., *Fulton et al*., 2013] and thus impact the organic reactivity [*Savage et al*., 2014], though only at spatial scales of millimeters to centimeters from the fault slip plane [e.g., *Fulton et al*., 2010; *Fulton and Harris*, 2012]. Such frictional heating from earthquake rupture that reached the frontal part of the Nankai prism was inferred using vitrinite reflectance data [*Sakaguchi et al*., 2011]. However, localized fluid flow is still needed to explain temperature changes (around 5°C or higher) over a distance greater than a few centimeters from the fault plane to account for the reactivation of organic matter resulting in the observed geochemical profiles.

In addition to frictional heating, earthquakes and aftershocks can cause a change in permeability and, consequentially, increase the hydraulic diffusivity for example by breaking up permeability-limiting fine-grained deposits [e.g., *Manga et al*., 2003; *Manga et al*., 2012; *Candela et al*., 2014]. Such a permeability change in the accretionary prism sediments can favor the channeling of flow parallel to fault structure [*Ikari and Saffer*, 2012]. Deformation can open permeability and lead to changes in the pressure regimes that can cause fluid squeezing and consequently advective fluid flow. At Hole C0007D, *Ikari and Saffer* [2012] discuss a permeability increase, which could allow a (lateral) fluid flow on small scale. At Site C0006, two concentrated deformation zones were identified in the lower core deposits (at 433.75–440.00 and 526–545 mbsf), with tectonic breccia observed at about 440 mbsf. Similar observations have been made on the Alpine Fault (New Zealand), where fluid flow occurs along the higher-permeability damage zone on both sides of the gouge zone [*Sutherland et al*., 2012]. After heat diffusion in thin low-permeability layers (the gouge zone) reaches the damage zone, the heat could be further transported by advective fluid flow away from this zone.

Many deformation structures were described in the sediment core around 460–490 mbsf, with an abundance of small fractures [*Kinoshita et al*., 2009]. These could allow potential discrete fluid flow pathways. The observed isotope excursion falls just below the upper deformed zone in this fractured zone (Figure 8). Some fraction of the coseismic frictional heating-induced temperature increase of up to 300°C [*Sakaguchi et al*., 2011; *Fulton and Harris*, 2012] could be transported within fluids along those fractures. The flow of heated fluids along the damage zone would lead to a localized thermal elevation and thus a temperature increase of the surrounding environment of a few °C for a short period of time. The lack of geochemical observations indicative of flow from depth suggest that this fluid flow occurs over a short distance or along concentration contours.

Although we do not know the exact mechanism that would cause a localized thermal perturbation, a combination of frictional heating and advective fluid flow appears to be the most reasonable scenario for a short-term temperature excursion over a narrow sediment interval at our investigated sites. Such a

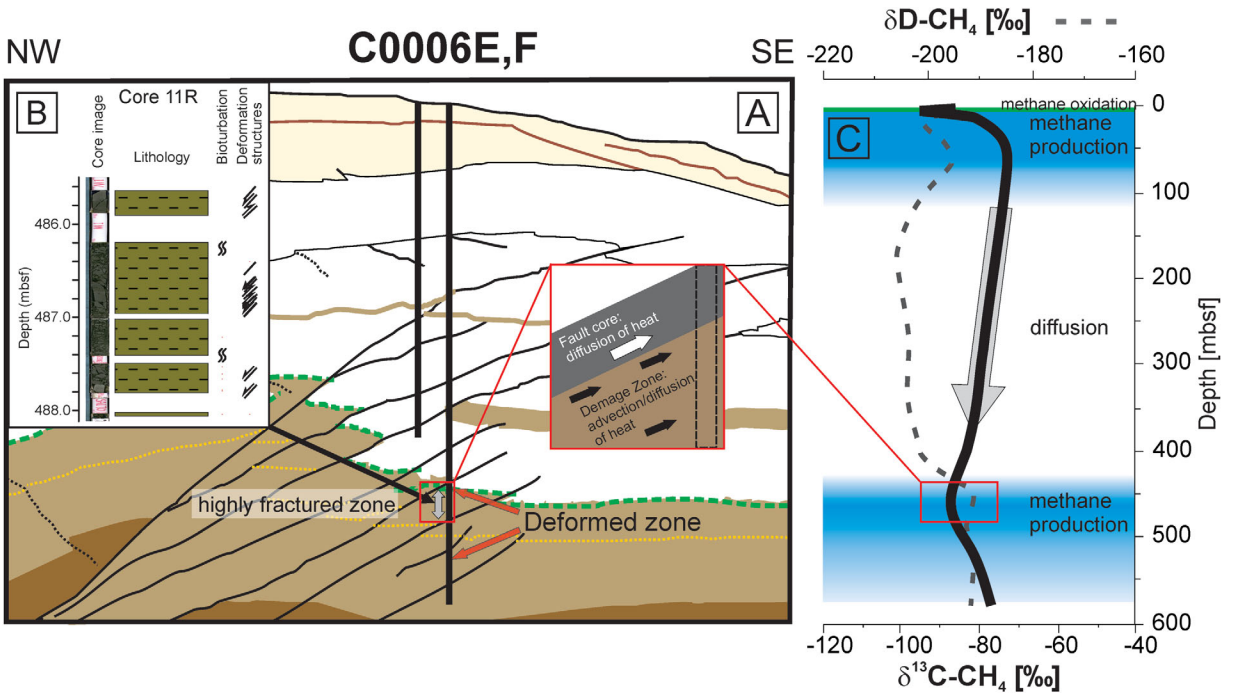

Figure 8. Schematic geochemical profiles with potential biogeochemical processes and structural features at Site C0006. (a) Simplified structural overview and transport mechanisms related to the zone of carbon isotope excursion (red square). (b) Lithology and sediment description of Core 11R [after *Kinoshita et al.*, 2009] as an example of the highly fractured sediment layers below a major deformation zone. (c) Simplified geochemical profile of $\delta^{13}C\text{-}CH_4$ (blue line) and $\delta D\text{-}CH_4$ (gray dashed line) and zones of potential biogeochemical processes.

temperature rise would lead to an increase of organic matter reactivity/bioavailability [*Parkes et al.*, 1989]. The subsequent generation of organic substrates [*Parkes et al.*, 1989] could explain the stimulation of microbial activity via a new supply of energy [*Wellsbury et al.*, 1997; *Parkes et al.*, 2006] in these deep marine sediments (Figure 8).

4. Summary and Conclusions

The data from sediments at IODP Site C0008 show a classic isotope profile for methane, with almost no variation throughout the deeper sediment column, while at Sites C0006 and C0007 the methane isotope composition indicates active methanogenesis occurring several hundreds of meters below the seafloor (Figures 2–4). The concurrent increase in total alkalinity concentration and decrease in C-isotope values indicates methane production in deep-subsurface sediments. After considering the full range of possibilities, we attribute the active microbial carbon cycling at the toe of the accretionary prism to either substrate delivery to the microbial community by fluid flow or as a result of reactivated organic matter via a transient increase in temperature. Both scenarios require tectonic activity that we relate to seismicity, though we acknowledge ambiguity in the actual mechanism that causes a temperature increase of a few °C over several meters and the related organic matter reactivation, i.e., the energy source for the microbial activity. Nevertheless, the application of a numerical model suggests that the tectonic event occurred a few hundred years ago (in the range of 200–400 years). Although the model is based on several assumptions, our estimate remains robust for various rate scenarios—placing the event into recent historical time frames. Two historically documented earthquakes occurred within this time frame suggested by our numerical model results: the multi-segment mega Hoei-earthquake in 1707 [*Ando*, 1975] and the comparably smaller 1605 Keicho earthquake with known, exceptionally large tsunami. This suggests the possibility that at least one of these events slipped to the trench at the Nankai and was responsible for the transient heating that resulted in the observed methane C-isotope excursion.

Moreover, the tectonic impact on the carbon cycle might influence the application of carbon paleo-proxies. Although in young sediments the production of methane and consequent enrichment of the residual organic matter in ^{13}C has no significant impact on the bulk organic isotope signal [*Boehme et al.*, 1996], the

change of the isotopic composition of organic matter during constant degradation with depth and even reactivation could have an impact on the buried and preserved carbon isotope signal. For example, the released dissolved inorganic carbon during the organic matter mineralization could overprint the C-isotopic signature of carbonates precipitated during early diagenesis. The influence on the isotopic signal thus might not only impact the interpretation for the origin of organic matter and/or carbonates in ancient rocks but could also be a powerful tool to diagnose and constrain the timing of young tectonic events. Furthermore, the associated methane isotope excursion could be used to pin down ongoing microbial activity in deep biosphere environments—thus providing a potential road map for further and more detailed microbial investigations.

Acknowledgments

The authors thank the captain and the crew of the D/V Chikyu during IODP Expedition 316. Our special appreciation goes to L. Wehrmann, T. Ferdelman, and M. Formolo for fruitful discussions and critical comments. We thank the Editor and two reviewers for providing constructive comments that helped to improve this paper. This research was funded by the Deutsche Forschungsgemeinschaft (DFG)-IODP and the National Science Foundation (NSF). N.R. was partially supported by the Max Planck Society. M.S. acknowledges support by Swiss National Science Foundation (grant PP00P2-133481). E.S. acknowledges support from the U.S. Science Support Program and NSF (OCE-0751497). R.H. was partially supported by U.S. Science Support Program for IODP (NSF 0652315) that is administered by the Consortium for Ocean Leadership. This is an Oklahoma State University-Boone Pickens School of Geology contribution 2015-27. This research used samples and data provided by the Integrated Ocean Drilling Program (IODP). All additional data are provided in the supporting information.

References

Adler, M., C. Hensen, F. Wenzhöfer, K. Pfeifer, and H. D. Schulz (2001), Modeling of subsurface calcite dissolution by oxic respiration in supralysoclinal deep-sea sediments, *Mar. Geol.*, *177*, 167–189.

Alperin, M. J., W. S. Reeburgh, and M. J. Whiticar (1988), Carbon and hydrogen isotope fractionation resulting from anaerobic methane oxidation, *Global Biogeochem. Cycles*, *2*, 279–288.

Ando, M. (1975), Source mechanisms and tectonic significance of historical earthquakes along the Nankai Trough, Japan, *Tectonophysics*, *27*, 119–140.

Arning, E. T., Y. Fu, W. van Berk, and H.-M. Schulz (2011), Organic carbon remineralisation and complex, early diagenetic solid–aqueous solution–gas interactions: Case study ODP Leg 204, Site 1246 (Hydrate Ridge), *Mar. Chem.*, *126*, 120–131, doi:10.1016/j.marchem.2011.04.006.

Blair, N. (1998), The δ^{13}C of biogenic methane in marine sediments: The influence of C deposition rate, *Chem. Geol.*, *152*, 139–150.

Boehme, S. E., N. E. Blair, L. Jeffrey, P. Chanton, and C. S. Martens (1996), A mass balance of ^{13}C and ^{12}C in an organic-rich methane-producing marine sediment, *Geochim. Cosmochim. Acta*, *60*, 3835–3848.

Boudreau, B. P. (1997), Diagenetic Models and Their Implementation: Modelling Transport and Reactions in Aquatic Sediments, Springer.

Burdige, D. J. (2011), Temperature dependence of organic matter remineralization in deeply-buried marine sediments, *Earth Planet. Sci. Lett.*, *311*, 396–410.

Candela, T., E. E. Brodsky, C. Marone, and D. Elsworth (2014), Laboratory evidence for particle mobilization as a mechanism for permeability enhancement via dynamic stressing, *Earth Planet. Sci. Lett.*, *392*, 279–291, doi:10.1016/j.epsl.2014.02.025.

Canfield, D. E. (1994), Factors influencing organic-carbon preservation in marine sediments, *Chem. Geol.*, *114*, 315–329.

de Leeuw, J. W., and C. Largeau (1993), A review of macromolecular organic compounds that comprise living organisms and their role in kerogen, coal and petroleum formation, in *Organic Geochemistry*, edited by M. H. Engel and S. A. Macko, pp. 23–72, Plenum, N. Y.

Dugan, B., and H. Daigle (2011), Data report: Permeability, compressibility, stress state, and grain size of shallow sediments from Sites C0004, C0006, C0007, and C0008 of the Nankai accretionary complex, *Proc. Integrated Ocean Drill. Program*, *314–316*, doi:10.2204/iodp.proc.314315316.211.2011.

Emerson, S., V. Grundmanis, and D. Graham (1982), Carbonate chemistry in marine pore waters: MANOP sites C and S, *Earth Planet. Sci. Lett.*, *61*, 220–232.

Expedition 316 Scientists (2009), Expedition 316 Site C0006, *Proc. Integrated Ocean Drill. Program*, *314–316*, doi:10.2204/iodp.proc.314315316.134.2009.

Fulton, P. M., and R. N. Harris (2012), Thermal considerations in inferring frictional heating from vitrinite reflectance and implications for shallow coseismic slip within the Nankai Subduction Zone, *Earth Planet. Sci. Lett.*, *335–336*, 206–215.

Fulton, P. M., R. N. Harris, D. M. Saffer, and E. E. Brodsky (2010), Does hydrologic circulation mask frictional heat on faults after large earthquakes?, *J. Geophys. Res.*, *115*, B09402, doi:10.1029/2009JB007103.

Fulton, P. M., et al. (2013), Low coseismic friction on the Tohoku-Oki Fault determined from temperature measurements, *Science*, 6, 1214–1217.

Gieskes, J. M., and J. R. Lawrence (1981), Alteration of volcanic matter in deep sea sediments: Evidence from the chemical composition of interstitial waters from deep sea drilling cores, *Geochim. Cosmochim. Acta*, *45*, 1687–1703.

Harris, R. N., F. Schmidt-Schierhorn, and G. Spinelli (2011), Heat flow along the NanTroSEIZE transect: Results from IODP Expeditions 315 and 316 offshore the Kii Peninsula, Japan, *Geochem. Geophys. Geosyst.*, *12*, Q0AD16, doi:10.1029/2011GC003593.

Hedges, J. I., and R. G. Keil (1995), Sedimentary organic matter preservation: An assessment and speculative synthesis, *Mar. Chem.*, *4*, 81–115.

Hensen, C., M. Zabel, K. Pfeifer, T. Schwenk, S. Kasten, N. Riedinger, H. D. Schulz, and A. Boetius (2003), Control of sulfate pore-water profiles by sedimentary events and the significance of anaerobic oxidation of methane for burial of sulfur in marine sediments, *Geochim. Cosmochim. Acta*, *67*, 2631–2647.

Hirose, T., S. Kawagucci, and K. Suzuki (2011), Mechanoradical H_2 generation during simulated faulting: Implications for an earthquake-driven subsurface biosphere, *Geophys. Res. Lett.*, *38*, L17303, doi:10.1029/2011GL048850.

Holm, N. G., and J. L. Charlou (2001), Initial indications of abiotic formation of hydrocarbons in the Rainbow ultramafic hydrothermal system, Mid-Atlantic Ridge, *Earth Planet. Sci. Lett.*, *191*, 1–8.

Ikari, M. J., and D. M. Saffer (2012), Permeability contrasts between sheared and normally consolidated sediments in the Nankai accretionary prism, *Mar. Geol.*, *295–298*, 1–13, doi:10.1016/j.margeo.2011.11.006.

Inagaki, F., M. Suzuki, K. Takai, H. Oida, T. Sakamoto, K. Aoki, K. H. Nealson, and K. Horikoshi (2003), Microbial communities associated with geological horizons in coastal subseafloor sediments from the sea of Okhotsk, *Appl. Environ. Microbiol.*, *69*, 7224–7235.

Inagaki, F., et al. (2015), Exploring deep microbial life in coal-bearing sediment down to ~2.5 km below the ocean floor, *Science*, *349*, 420–424, doi:10.1126/science.aaa6882.

Jørgensen, B. B., and S. D'Hondt (2006), A starving majority deep beneath the seafloor, *Science*, *314*, 932–934.

Kinoshita, M., H. Tobin, J. Ashi, G. Kimura, S. Lallemant, E. J. Screaton, D. Curewitz, H. Masago, K. T. Moe, and the Expedition 314/315/316 Scientists (2009), NanTroSEIZE Stage 1: Investigations of seismogenesis: Nankai Trough, Japan, *Proc. Integrated Ocean Drill. Program*, 314–316.

Lettmann, K. A., N. Riedinger, R. Ramlau, N. Knab, M. E. Böttcher, A. Khalili, J.-O. Wolff, and B. B. Jørgensen (2012), Estimation of biogeochemical rates from concentration profiles: A novel inverse method, *Estuarine Coastal Shelf Sci.*, *100*, 26–37, doi:10.1016/j.ecss.2011.01.012.

Lin, L. H., G. F. Slater, B. S. Lollar, G. Lacrampe-Couloume, and T. C. Onstott (2005), The yield and isotopic composition of radiolytic H_2, a potential energy source for the deep subsurface biosphere, *Geochim. Cosmochim. Acta*, *69*, 893–903.

Lovley, D. R., D. F. Dwyer, and M. J. Klug (1982), Kinetic analysis of competition between sulfate reducers and methanogens for hydrogen in sediments, *Appl. Environ. Microbiol.*, *43*, 1373–1379.

Manga, M., E. E. Brodsky, and M. Boone (2003), Response of stream flow to multiple earthquakes, *Geophys. Res. Lett.*, *30*(5), 1214, doi:10.1029/2002GL016618.

Manga, M., I. Beresnev, E. E. Brodsky, J. E. Elkhoury, D. Elsworth, S. E. Ingebritsen, D. C. Mays, and C.-Y. Wang (2012), Changes in permeability caused by transient stresses: Field observations, experiments, and mechanisms, *Rev. Geophys.*, *50*, RG2004, doi:10.1029/2011RG000382.

Martens, C. S., and R. A. Berner (1974), Methane production in the interstitial waters of sulfate-depleted marine sediments, *Science*, *185*, 1167–1169.

Moore, G. F., et al. (2009), Structural and seismic stratigraphic framework of the NanTroSEIZE Stage 1 transect, *Proc. Integrated Ocean Drill. Program*, 314–316, doi:10.2204/iodp.proc.314315316.102.2009.

Moore, G. F., B. B. Boston, M. Strasser, M. B. Underwood, and R. A. Ratliff (2015), Evolution of tectono-sedimentary systems in the Kumano Basin, Nankai Trough forearc, *Mar. Pet. Geol.*, *67*, 604–616.

Newberry, J. C., G. Webster, B. A. Cragg, R. J. Parkes, A. J. Weightman, and J. C. Fry (2004), Diversity of prokaryotes and methanogenesis in deep subsurface sediments from the Nankai Trough, Ocean Drilling Program Leg 190, *Environ. Microbiol.*, *6*, 274–287, doi:10.1111/j.1462-2920.2004.00568.x.

Parkes, R. J., G. R. Gibson, I. Mueller-Harvey, W. J. Buckingham, and R. A. Herbert (1989), Determination of the substrates for sulphate-reducing bacteria within marine and estuarine sediments with different rates of sulphate reduction, *Microbiology*, *135*, 175–187.

Parkes, R. J., B. A. Cragg, J. C. Fry, R. A. Herbert, J. W. T. Wimpenny (1990), Bacterial biomass and activity in deep sediment layers from the Peru margin, *Philos. Trans. R Soc. Lond. A.*, *331*, 139–153.

Parkes, R. J., P. Wellsbury, I. D. Mather, S. J. Cobb, B. A. Cragg, E. R. C. Hornibrook, and B. Horsfield (2006), Temperature activation of organic matter and minerals during burial has the potential to sustain the deep biosphere over geological timescales, *Org. Geochem.*, *38*, 845–852.

Pimmel, A., and G. Claypool (2001), Introduction to shipboard organic geochemistry on the JOIDES resolution, *ODP Tech. Note 30*, Ocean Drill. Program, College Station, Tex. [Available at http://www-odp.tamu.edu/publications/tnotes/tn30/INDEX.]

Pohlman, J. W., M. Kaneko, V. B. Heuer, R. B. Cofin, and M. Whiticar (2009), Methane sources and production in the northern Cascadia margin gas hydrate system, *Earth Planet. Sci. Lett.*, *287*, 504–512.

Riedinger, N., and B. Brunner (2014), Data report: Concentration and sulfur isotope composition of iron monosulfide and pyrite from sediments collected during IODP expedition 316, Nankai Trough, Japan, *Proc. Integrated Ocean Drill. Program*, 314–316, doi:10.2204/iodp.proc.314315316.223.2014.

Riedinger, N., B. Brunner, M. J. Formolo, E. Solomon, S. Kasten, M. Strasser, and T. G. Ferdelman (2010), Oxidative sulfur cycling in the deep biosphere of the Nankai Trough, Japan, *Geology*, *38*, 851–854.

Roussel, E. G., M. A. Cambon-Bonavita, J. Querellou, B. A. Cragg, G. Webster, D. Prieur, and R. J. Parkes (2008), Extending the sub-sea-floor biosphere, *Science*, *320*, 1046, doi:10.1126/science.1154545.

Rowe, K., E. Screaton, J. Guo, and M. B. Underwood (2011), Data report: Permeabilities of sediments from the Kumano Basin transect off Kii Peninsula, Japan, *Proc. Integrated Ocean Drill. Program*, 314–316, doi:10.2204/iodp.proc.314315316.211.2011.

Sakaguchi, A., et al. (2011), Seismic slip propagation to the updip end of plate boundary subduction interface faults: vitrinite reflectance geothermometry on Integrated Ocean Drilling Program NanTroSEIZE cores, *Geology.*, *39*, 395–398, doi:10.1130/G31642.1.

Savage, H. M., P. J. Polissar, R. Sheppard, C. D. Rowe, and E. E. Brodsky (2014), Biomarkers heat up during earthquakes: New evidence of seismic slip in the rock record, *Geology*, *42*, 99–102, doi:10.1130/G34901.1.

Screaton, E. J., G. Kimura, D. Curewitz, and the Expedition 316 Scientists (2009a), Expedition 316 summary, *Proc. Integrated Ocean Drill. Program*, 314–316, doi:10.2204/iodp.proc.314315316.131.2009.

Screaton, E., G. Kimura, D. Curewitz, and the Expedition 316 Scientists (2009b), Interactions between deformation and fluids in the frontal thrust region of the NanTroSEIZE transect offshore the Kii Peninsula, Japan: Results from IODP Expedition 316 Sites C0006 and C0007, *Geochem. Geophys. Geosyst.*, *10*, Q0AD01, doi:10.1029/2009GC002713.

Shipboard Scientific Party (2003), Explanatory notes, in *Controls on Microbial Communities in Deeply Buried Sediments, Eastern Equatorial Pacific and Peru Margin Sites 1225-1231, Proc. Ocean Drill Program Initial Rep.*, vol. 201, edited by S. L. D'Hondt, et al., U.S. Gov. Print. Off., Washington, D. C.

Sivan, O., D. P. Schrag, and R. W. Murray (2007), Geochemistry of methane in marine sediments Rates of methanogenesis and methanotrophy in deep-sea sediments, *Geobiology*, *5*, 141–151.

Strasser, M., et al. (2009), Origin and evolution of a splay fault in the Nankai accretionary prism, *Nat. Geosci.*, *2*, 648–652.

Surdam, R. C., and L. J. Crossey (1985), Organic–inorganic reactions during progressive burial: Key to porosity and permeability enhancement and preservation, *Philos. Trans. R. Soc. London A*, *315*, 135–156.

Sutherland, R., et al. (2012), Drilling reveals fluid control on architecture and rupture of the Alpine fault, New Zealand, *Geology*, *40*, 1143–1146, doi:10.1130/G33614.1.

Underwood, M. B., and G. F. Moore (2011), Evolution of sedimentary environments in the subduction zone v of Southwest Japan: Recent results from the NanTroSEIZE Kumano Transect, in *Tectonics of Sedimentary Basins: Recent Advances*, edited by C. Busby and A. Azor, pp. 310–326, John Wiley, Chichester, U. K., doi:10.1002/9781444347166.ch15.

Underwood, M. B., G. F. Moore, A. Taira, A. Klaus, M. E. J. Wilson, C. L. Fergusson, S. Hirano, J. Steurer, and the Leg 190 Shipboard Scientific Party (2003), Sedimentary and tectonic evolution of a trench-slope basin in the Nankai subduction zone of southwest Japan, *J. Sediment. Res.*, *73*, 589–602.

Wallace, P. J., G. R. Dickens, C. K. Paull, and W. Ussler (2000), Effects of core retrieval and degassing on the carbon isotope composition of methane in gas hydrate—and free gas—bearing sediments from the Blake Ridge, *Proc. Ocean Drill. Program Sci. Results*, *164*, doi:10.2973/odp.proc.sr.164.209.2000.

Wehrmann, L. M., et al. (2011), Coupled organic and inorganic carbon cycling in the deep subseafloor sediment of the northeastern Bering Sea slope (IODP Exp. 323), *Chem. Geol.*, *284*, 251–261, doi:10.1016/j.chemgeo.2011.03.002.

Wellsbury, P., K. Goodman, T. Barth, B. A. Cragg, S. P. Barnes, and R. J. Parkes (1997), Deep marine biosphere fuelled by increasing organic matter availability during burial and heating, *Nature*, *388*, 573–576.

Westrich, J. T., and R. A. Berner (1984), The role of sedimentary organic matter in bacterial sulfate reduction: The G model tested, *Limnol. Oceanogr.*, *29*, 236–249.

Whiticar, M. J. (1999), Carbon and hydrogen isotope systematics of bacterial formation and oxidation of methane, *Chem. Geol.*, *161*, 291–314.

Whiticar, M. J., E. Faber, and M. Schoell (1986), Biogenic methane formation in marine and freshwater environments: CO_2 reduction vs acetate fermentation–isotope evidence, *Geochim. Cosmochim. Acta*, *50*, 693–709.

Wolf-Gladrow, D. A., R. E. Zeebe, C. Klaas, A. Kortzinger, and A. G. Dickson (2007), Total alkalinity: The explicit conservative expression and its application to biogeochemical processes, *Mar. Chem.*, *106*, 287–300.

Yamaguchi, A., S. F. Cox, G. Kimura, and S. Okamoto (2011), Dynamic changes in fluid redox state associated with episodic fault rupture along a megasplay fault in a subduction zone, *Earth Planet. Sci. Lett.*, *302*, 369–377.

Yoshinaga, M. Y., T. Holler, T. Goldhammer, G. Wegener, J. W. Pohlman, B. Brunner, M. M. M. Kuypers, K.-U. Hinrichs, and E. Marcus (2014), Carbon isotope equilibration during sulphate-limited anaerobic oxidation of methane, *Nat. Geosci.*, *7*, 190–194, doi:10.1038/ngeo2069.

Yoshioka, H., S. Sakata, B. A. Cragg, R. J. Parkes, and T. Fujii (2009), Microbial methane production rates in gas hydrate-bearing sediments from the eastern Nankai Trough, off central Japan, *Geochem. J.*, *43*, 315–321.